Journal of Ovonic Research Vol. 22, No. 3, May– June 2026, p. 112-125

Original Research

Temperature Effect on Structural, Optical and Magnetic Properties of Sol-Gel Prepared Bismuth Ferrite Nanopowder

Aliaa M. Zaki [1], Nasma A. Jaber [1], Ghaiath A. Fadhil [2,*]

[1] Medical Physics Department, College of Science, Al-Karkh University of Science, Baghdad, Iraq;
[2] College of Engineering, Al-Karkh University of Science, Baghdad, Iraq.
* Correspondence: ghaiath.fadhil@kus.edu

Received: February 12, 2026; Accepted: April 29, 2026

Abstract: Bismuth Ferrite ($BiFeO_3$) nanoparticles were synthesized through the sol-gel technique at 180 °C and annealed at 400, 600, and 800 °C to study the influence of thermal treatment on their structural, optical and magnetic properties. These nanoparticles have multiferroic properties at room temperature and are advantageous in a wide range of applications. The structural characterization using X-ray diffraction confirmed the rhombohedral perovskite crystal structure in all samples but with an increase in crystallite size and a decrease in X-ray density with increasing annealing temperature. The Raman spectroscopy analysis revealed vibrational modes that characteristics to $BiFeO_3$ with peak shifts and widening as the annealing temperature increases. The optical properties of the annealed $BiFeO_3$ nanoparticles showed a red shift in absorption characteristics and a decrease in the energy bandgap from 2.9 eV to 2.4 eV as a result of the enhanced crystallinity. The magnetic behavior of $BiFeO_3$ revealed soft magnetic characteristics and a reduction in the saturation magnetization with annealing temperature increase, reaching a value of 0.25 emu/g at 800 °C. The hysteresis loops demonstrate that $BiFeO_3$ nanoparticles deviate from their room temperature multiferroic behavior toward paramagnetic behavior as the annealing temperature increases. These insights are essential for $BiFeO_3$ nanoparticles potential use in optoelectronic and photocatalytic applications.

Keywords: Bismuth; Band gap; Temperature control; Rhombohedral; X-Rays; Sol-Gels.

1. Introduction

Multiferroic materials have both magnetic and ferroelectric order in the same phase [1]. At room temperature, these materials may show the magnetoelectric (ME) effect. This phenomenon is defined as polarization by a magnetic field or induction of magnetization by an electric field. Due to their advantages, multiferroic materials have attracted increasing research efforts [1]. A noticeable shortcoming of these multiferroics is the poor ferroic properties at ambient temperature. This issue has hindered the possibility of employing ferroic materials in various applications. The ABO_3 type of bismuth ferrite is a perovskite structure. In this structure, a Bi cation in a 3+ oxidation state occupies the A-site, a Fe cation in a 3+ oxidation state occupies the B-site, and an anion in a 2- oxidation state occupies the O-site. Six oxygen anions surround the Fe cations, creating octahedral coordination. The larger-size Bi-cations are enclosed by twelve oxygen anions, making a cuboctahedral arrangement [2]. $BiFeO_3$ has received significant attention since it is thought to have stable multiferroic characteristics at room temperature [3-5]. Bismuth ferrite has an antiferromagnetic Néel temperature of 370 °C. Below this temperature, $BiFeO_3$ becomes antiferromagnetic. This configuration breaks down and the material turns paramagnetic above 370 °C. $BiFeO_3$ is ferroelectric (having spontaneous electric

https://doi.org/10.15251/JOR.2026.223.112

polarization) below its ferroelectric Curie temperature of 830 °C. Above this temperature, the ferroelectric property vanishes and the material becomes paraelectric [3]. Bismuth ferrite has various applications in the fields of digital recording, radio, television, microwave, and satellite communications industries [3-6]. However, its principal use in multiferroics is limited by multiple drawbacks, including: the formation of secondary phases during the synthesis process, low magnetic properties, weak magnetoelectric coupling coefficients, broad range of ferroic transition temperatures and large leakage current [3]. Multiferroics can be either single-phase or composite materials. Single-phase multiferroics exhibit at least two ferroic characteristics at the same phase. On the other hand, composites are multiphase systems with distinct ferroic properties at each phase. In composite multiferroics, magnetoelectric coupling occurs indirectly through strain-mediated interactions. In contrast, the coupling occurs in single-phase multiferroics through the interaction of the magnetic and ferroelectric orders. Hence, the magnetic nature of these multiferroics could be controlled by electric field depending on the nature of their intrinsic coupling [3].

The development of the pure phase of $BiFeO_3$ is significantly influenced by the annealing temperature. Additionally, the annealing temperature affects the multiferroic materials' optical, magnetic, structural, and morphological characteristics [4]. The optical characteristics of bismuth ferrite exhibit the most notable impact of the annealing temperature. In previous studies, an annealing temperature between 600 and 850 °C was used in the preparation of bismuth ferrite. These temperatures are reported to be suitable for reducing the band gap. The obtained energy gap values ranged between 1.5 and 1.9 eV [5]. It is revealed that the band gap values decreased from 2.7 eV to 2.6 eV with temperature increased from 200 °C to 500 °C, indicating a change in the rate of electron-hole recombination. The electron-hole pairs in $BiFeO_3$ thin film can be stimulated by a photon with a wavelength of 580 nm. These photo-generated carriers move along domain boundaries at higher wavelengths during annealing process. It is found that annealing is a more effective method for enhancing crystallinity and reducing impurities in $BiFeO_3$ thin films [6]. Homogeneous $BiFeO_3$ nanopowder was prepared via the sol-gel approach at 550 °C [7]. The X-ray analysis confirmed that Bismuth Ferrite has a stable perovskite structure represented by a rhombohedral shape with a space group R3C. It was also revealed that high calcination temperatures are important for promoting the growth of bismuth ferrite crystals and preventing any impurity phases that may develop. These findings support other studies that suggested elevated temperatures affect optical properties. These characteristics suggest that bismuth ferrite is a suitable material for opto-electronics and infrared detectors because of its high refractive index and direct band [7]. The optical band analysis revealed that, due to the quantum size effect, the band value in the gap decreased as the calcination temperature increased. This phenomenon causes the energy gap values to decrease as the nanoparticle size increases. Bismuth ferrites can be employed as a photocatalyst to break down industrial effluents under visible light. Additionally, the pure phase of $BiFeO_3$ nanoparticles may find usage in optoelectronic systems [8]. The influence of annealing temperature on optical, magnetic, and structural characteristics was investigated in this study. A compound of bismuth ferrite made by the Sol-Gel technique, spontaneous combustion, was annealed at different temperatures (180, 400, 600 and 800 °C). The annealing temperature is varied to outline the role of structural phases on the resulting $BiFeO_3$ nanoparticles. An analysis of the energy bandgap and magnetic properties of the resulted nanoparticles is performed. The results obtained may shed a light on the possibility of fabricating bismuth ferrite nanoparticles that are useful in optoelectronic applications. Since $BiFeO_3$ loses its magnetic properties at elevated temperatures, it can also be manifested in applications that require superparamagnetic characteristics. This includes materials for drug delivery, biosensors, hyperthermia therapy and photocatalysts [9].

2. Materials and methods

2.1. Materials

The Bismuth Ferrite ($BiFeO_3$) powder was prepared by the following materials: Iron Nitrate $Fe(NO_3)_3$ 9(H Bismuth Nitrate $Bi(NO_3)_35H_2O$, citric acid ($C_6H_8O_7$ H_2O), Ammonia solution (NH_4OH), and distilled Water. The molar mass of each material calculated from its stoichiometric weight percentage where: one mole of Bi nitrate, two moles of Fe nitrate and three moles of citric acid. Because it prevents ions from settling out, helps mix the solution thoroughly, and reduces the temperature at which crystals form, citric acid is employed as a catalyst [10].

2.2. Method

Due to its benefits, such as its high reactivity rate, low reaction temperature requirements, and ability to produce tiny particles, the sol-gel process is frequently employed to prepare a variety of compounds, including ferrites [11, 12]. 3.9 gm of bismuth nitrate were mixed with 6.5 g of iron nitrate and 5.1 g of Citric Acid and dissolved in 80 ml of Distilled Water. The solution is left to homogenize for one hour at room temperature by using the magnetic hot plate stirrer model SH-2 at high rotation speed. Then a 10 ml of ammonia solution was mixed with solution to equalize it until the pH value became equal to 7 with continuous stirring. After 10 minutes, we raise the temperature to 80 degrees Celsius for 4 hours while continuing to stir. This leads to the liquid solution turning into a viscous solution with a high density, which is known as gel. A fluffy, loose structure was formed by burning the gel in a self-propagating combustion manner until all the gel was burned off. This structure was then crushed to produce Bi ferrite powder. This powder was annealed afterwards at temperatures of 400, 600, and 800 °C for one hour each with vacuum. Figure 1 shows the preparation procedure described above.

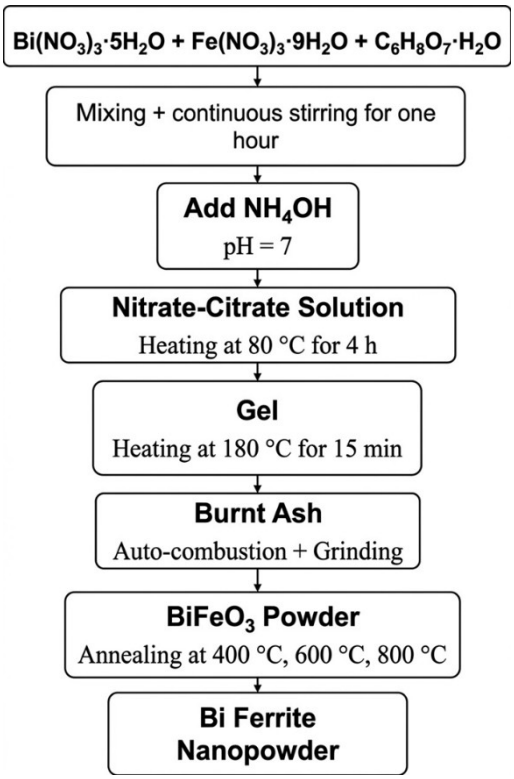

Figure 1. Preparation procedure of $BiFeO_3$ nanopowder using the sol-gel method.

2.3. Characterization

The samples were examined utilizing a Rigaku Ultima IV X-ray diffractometer. The resulting X-ray diffraction patterns were refined using "Material Analysis Using Diffraction" (MAUD) program and Rietveld's

method for the structural analysis and cation distribution calculations. The sintered sample was subjected to Raman measurements using a Jobin-Ivon T64000 monochromator. A magnification microscope with a 100x magnification was utilized to focus 532 nm irradiation on the specimen using a Coherent Innova 99 Ar^+ laser. The backscattered light was collected using the same microscope. An apparatus for detecting charge-coupled devices picked up the scattered light. The spectral range of room temperature Raman spectra is 200–1000 cm^{-1}. The $BiFeO_3$ spectra of absorption were obtained via UV-Visible spectrophotometer. At room temperature, magnetic characterization is done using a vibrating sample magnetometer (VSM).

3. Results & discussion

3.1. X-Ray analysis

The X-ray diffraction analysis of $BiFeO_3$, prepared at T= 180 °C and annealed at 400, 600 and 800 °C for one hour is shown in Figure 2. The spectra of $BiFeO_3$, when compared to the standard ICSD card no.01-086-1518, revealed a rhombohedral phase with space group R3c [13, 14]. Secondary phases have been observed such as $Bi_2Fe_4O_9$ orthorhombic phase ICDD Card No. 98-002-6808 and $Bi_{25}FeO_{40}$ ICDD Card No. 01-078-1543 [15]. The increase in annealing temperature affects the bismuth ferrite nanopowder, causing a phase transition at 850 °C. This means bismuth ferrite can decompose into Fe_2O_3 and Bi_2O_3. The occurrence of secondary phases is a direct result of annealing the structure following the drying step of the sol-gel process, as demonstrated by previous studies [3, 16].

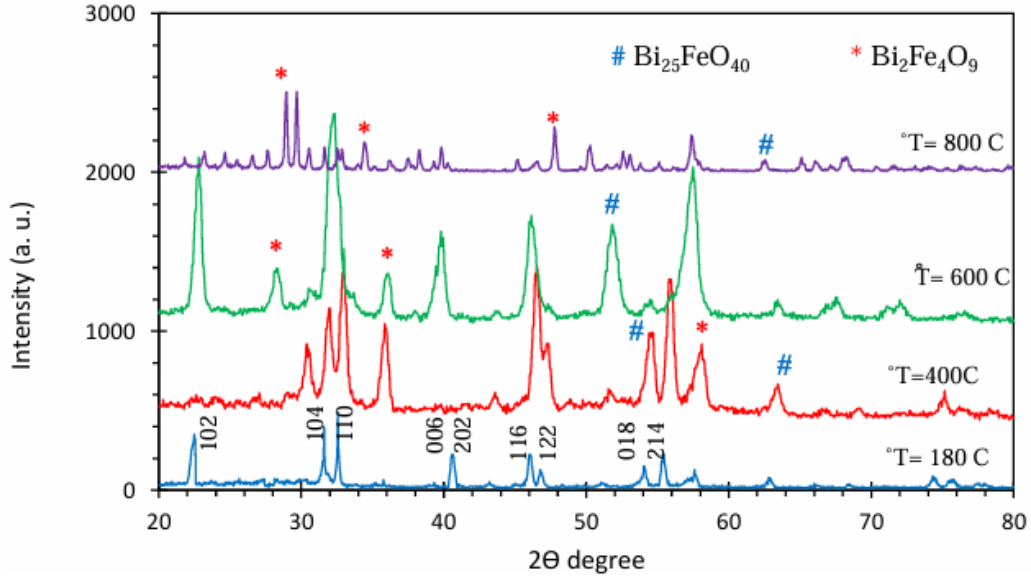

Figure 2. X-ray diffraction patterns of $BiFeO_3$ nanoparticles prepared at 180 °C and annealed at 400, 600 and 800 °C.

The quantitative analysis of the secondary phases is performed using the Rietveld Refinement method. The ratios for each phase, based on their intensity at the annealing temperatures, are noted in Table 1. At 180 °C, the sample has a high purity of bismuth ferrite phase. As the temperature rises, the amount bismuth ferrite phase decreases, and secondary phases become more noticeable due to bismuth evaporation and the formation of iron-rich phases [1].

Table 1. Quantitative phase analysis of $BiFeO_3$ nanoparticles prepared at 180 °C and annealed at 400, 600 and 800 °C.

Temperature (°C)	$BiFeO_3$ (%)	$Bi_2Fe_4O_9$ (%)	$Bi_{25}FeO_{40}$ (%)
400	41	31	28

600	38	32	30
800	31	36	33

Since the bismuth ferrite crystal has a specific structure, a perovskite rhombohedral R3c structure, the lattice constant value is calculated for two distinct axes. The lattice constant (a_1) evaluated by applying the formula (1) [17]:

$$\frac{1}{d^2}=\frac{3}{4}\left(\frac{h^2+hk+k^2}{a_l^2}\right)+\frac{l^2}{c^2} \quad (1)$$

Here, Miller indices are denoted by hkl, d is interplanar spacing. The lattice constant (a_l) is calculated for $h, k \neq 0$. Thus, we extract the value of (a_l) in the horizontal plane (1 1 0). In addition, the value of (c) is calculated for a vertical plane such as (0 0 4) from Equation (1) [18]. The Material Analysis Using Diffraction (MAUD) program and Rietveld refinement approach for structural analysis and cation distribution computations were used to refine the X-ray diffraction data. The values of the lattice constants of bismuth ferrite increases with the increasing annealing temperature (Table 2), which might be related to thermal expansion. The atoms in the crystal structure have a higher vibration when the temperature rises, which disturbs the interatomic distances. This thermal expansion may be asymmetric in all directions and therefore the lattice constants vary with the different crystal axes. Several studies have found that increasing the temperature to more than 850 °C causes the crystal phase to shift, such as the transition from the rhombohedral phase to other phases, such as orthorhombic or cubic. This results in a sudden or non-linear change in the lattice constant [19]. The size of the crystallite (D_{cs}) is determined in the horizontal plane (1 1 0) with higher intensity using Debye-Scherrer formula [1, 8]:

$$D_{cs}=\frac{0.94\,\lambda}{\beta\cos\theta} \quad (2)$$

λ is the wavelength of Cu-Kα (1.54 A°), β (FWHM in radians) is measured for various X-ray diffraction lines that correspond to the various planes, θ is the angle of Bragg diffraction, and 0.94 is a value that depends on the shape of lattice. As seen in Table 2, the crystallite size grows as the annealing temperature rises, which is in line with the findings of earlier research. The increase in crystallite size can result from several factors, including the rise in atomic energy caused by heat, which enhances their movement. This leads to the rearrangement of the atoms in the crystal sites, which enhances the growth of the grains and thus decreases the surface energy of the crystal [20]. The X-ray densities (d_{XRD}) were calculated [11]:

$$d_{XRD}=\frac{Z[M]}{N_A\ V} \quad (3)$$

Where: Z is the number of atoms per unit cell and equal to 6, [M] is the molecular weight, N_A is Avogadro's number and V is lattice volume for rhombohedral system is evaluated from the following equation [21]:

$$V=c\ \ a_l^2\ \ \frac{\sqrt{3}}{2} \quad (4)$$

The X-ray density values in Table 2 reveal a slight change in the calculated values due to the change in the values of the lattice constants. Previous studies indicate that this constant is a theoretical value that depends mainly on the crystal size, which is calculated from the values of the lattice constants (Table 3). These studies

also indicate that the effect of annealing temperature on X-ray density values is so small that it can be neglected [19-22].

Table 2. X-ray pattern analysis of $BiFeO_3$ nanoparticles annealed at different temperature.

T ˚C	$d_{(104)}$ (Å)	$d_{(110)}$ (Å)	a_1 (Å)	c (Å)	FWHM $\beta_{(110)}$ (deg)	$2\theta_{(110)}$ (deg)	d_{XRD} (g\cm^3)	D_{cs} (nm)
180	2.817	2.789	5.57	13.56	0.22	32.06	8.55	28.7
400	2.823	2.794	5.58	13.90	0.49	32.01	8.29	28.8
600	2.829	2.799	5.59	13.93	0.59	31.95	8.24	34.7
800	2.836	2.805	5.61	13.97	0.593	31.87	8.18	78.7

Table 3. X-ray pattern analysis of $BiFeO_3$ in previous studies.

T ˚C	**a (Å)**	**c (Å)**	**D_{cs} (nm)**	**Reference**
400-600	-	-	47-71	[3]
150-750	-	-	6-45	[8]
500-800	5.58	13.86	30-51	[19, 20]
550	5.57	13.86	40	[1]

3.2. Raman spectra

Raman spectroscopy was employed to analyze samples to evaluate changes in vibrations and the polarizability of molecules, as it can identify structural alterations in a wide variety of nano-sized materials [11]. Raman mode can be extremely sensitive to the spin correlations, which can be useful for explaining spin–phonon interactions. In magnetic nanomaterials such as $BiFeO_3$, optical phonon modes are probably impacted by exchange coupling between magnetic ions that take place at and below the temperatures of magnetic phase transitions. The spin–phonon interaction usually results in a characteristic temperature dependency of the Raman phonon frequency, linewidth, or integrated intensity. The departure of the Raman mode frequency from the anharmonicity at and below the magnetic phase transition can be used to evaluate the intensity of spin–phonon coupling in ferromagnets or antiferromagnets [23]. Figure 3 shows the Raman spectrum of $BiFeO_3$ prepared by the sol-gel technique at 180 °C and at varying temperatures, annealed (400, 600 and 800 °C). The group theory states that 13 Raman active modes (4A+9E) are found for $BiFeO_3$ with a deformed rhombohedral structure and an R3c space group [24]. These vibrational modes are phonon patterns that arise from the interaction of light and lattice vibrations in the crystal. The modes (A) represent non-degenerated modes when the atoms vibrate along the polar axis and represent the vibration of heavy bismuth ions (Bi^{3+}). While (E) modes refers to doubly degenerate modes, which are considered the lateral vibrations of (O^{3+}) ions. There are 10 Raman modes in the range from 100 - 800 cm^{-1} (Fig. 3). High intensity peaks relate to modes A_1, A_2 and A_3. The other peaks are weak in intensity and decrease with increasing temperature. These peaks are represented by the modes (E_1, E_2, E_3, E_4, A_4, E_5 and E_6). The values of all these modes are shown in Table 4. When comparing these values with values from previous studies, there is a noticeable shift in the peaks towards higher frequencies. At higher temperatures (T > 180 °C), the Raman bands become broader due to increased phonon–phonon interactions and structural disorder. This limits the accuracy of peak position determination. When the

temperature rises, the atomic bonds of the bismuth ferrite crystal lattice begin to vibrate, which leads to a slight decrease in the frequency of the Raman peaks and thus a shift of the peaks towards lower wavenumber (red shift). Furthermore, with increasing temperature, the peaks become wider due to atoms vibration. Peaks such as A_3, E_2, E_4, A_4, E_5 and E_6 may disappear at elevated temperatures above 180°C, because of changes in crystal structure or an increase in its disorder [25].

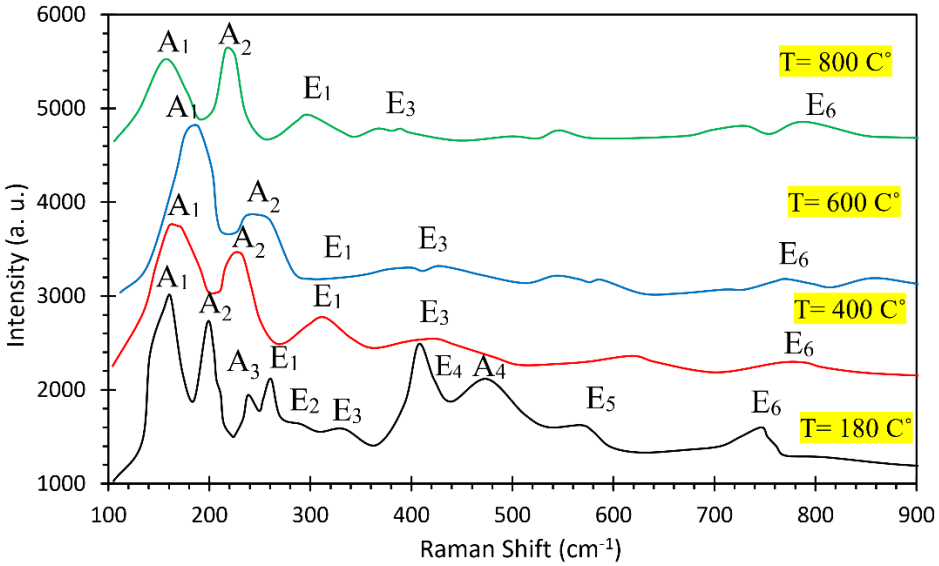

Figure 3. Raman spectra of $BiFeO_3$ prepared at 180 ˚C and annealed at 400, 600 and 800 °C.

Table 4. Raman modes for annealed $BiFeO_3$ nanoparticles in this study and previous studies.

Raman Modes	Position of Raman Shifts (cm^{-1})				Previous studies		
	T=180 ˚C	T=400 ˚C	T=600 ˚C	T=800 ˚C	T=550˚C Ref. [1]	T=450 ˚C Ref. [22]	T=550 ˚C Ref.[24],
A_1	160	164	186	158	136	146	138
A_2	196	228	235	218	170	175	171
A_3	239	311	329	297	217	219	217
E_1	265	388	406	363	260	261	261
E_2	295	420	428	390	278	282	275
E_3	335	442	444	466	345	332	346
E_4	410	545	557	498	365	367	372
A_4	472	593	615	543	425	435	429
E_5	569	623	732	599	469	480	470
E_6	740	783	785	692	520	550	520

3.3. UV-visible analysis

UV-visible spectra were utilized to investigate the optical characteristics (the absorbance and the energy band gap) of bismuth ferrite. Figure 4 illustrates the absorption spectrum of $BiFeO_3$ prepared at 180 °C and annealed at 400, 600, and 800 °C. The absorption band boundaries of $BiFeO_3$ were observed at 475.7 nm, 446.8 nm, 375.5 nm, and 356.3 nm, respectively. The highest absorption peak of $BiFeO_3$ nanoparticles is in the visible region. When the annealing temperature increases, these peaks diminish and appear at a lower wavelength (blue shift). This shift signifies a modification in the bandgap and electronic transition [26]. The peak at around

446.8 nm represents charge transfer at Fe-O band. The electrical transitions from valence-band oxide 2p states to conduction bands of iron 3d states were associated with the absorption band at 475.7 nm. The absorption of $BiFeO_3$ nanoparticles is more powerful in the visible portion of the spectrum than in the UV region; this is evidence of its potential use in solar cell applications [4].

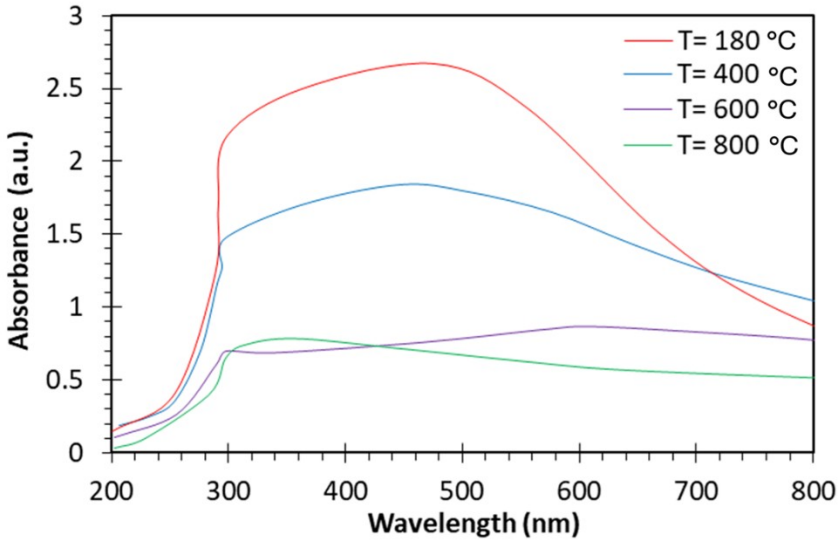

Figure 4. UV-visible spectra of $BiFeO_3$ nanoparticles prepared at 180 ˚C and annealed at 400, 600 and 800 °C.

The Tauc equation can be used to determine the energy band gap, or E_G [6,7,8]:

$$(\alpha h\nu)^2 = \delta(h\nu - E_G)^n \tag{5}$$

Where $h\nu$ is photon energy (ν: frequency of light, h: Planck constant), α is absorption coefficient, δ value is determined by the effective mass of the hole in the valence bands and the electron in the conduction bands. The kind of transition (optical or electron) is determined by n; a direct allowed transition occurs when n = 1/2, while a direct forbidden transition occurs when n = 3/2. n = 2 for indirect permitted transitions and n = 3 fat permits a linear adjustment is taken and extrapolated to theor indirect forbidden transitions. In $BiFeO_3$, the indirect band gap is represented by n = 2. The portion th abscissa axis to get the energy band gap [27, 28]. As the annealing temperature increases versus 180 ˚C to 800 ˚C, the energy bandgap values will fall from 2.9 eV to 2.4 eV (See Figure 5). This outcome is in line with the findings of earlier research [4, 6, 7, 8], as listed in Table 5.

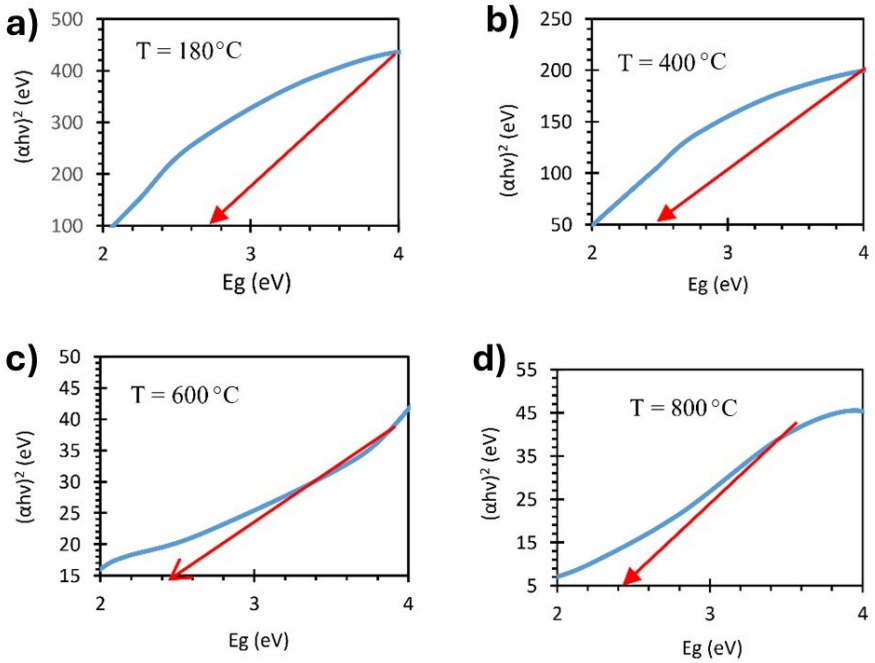

Figure 5. Energy bandgap (E_G) of $BiFeO_3$ nanoparticles a) prepared at 180 ˚C and annealed at b) 400 °C, c) 600 °C and d) 800 °C.

According to the X-ray analysis structure, the augmentation of crystallization followed by annealing may be the reason for the bandgap decrease after crystallization [6]. The presence of defect-induced energy levels within the bandgap, especially the energy levels near the conduction band edge, may contribute to the reduction in the optical bandgap. Note that electrons will be able to move between the conduction band and the valence band more efficiently if the bandgap is narrowed [28]. The results show that the optical bandgap and exponential optical absorption edge can be controlled by the degree of structural disorder in the $BiFeO_3$ lattice. The band gap value dropped at elevated temperatures. The intermediate energy level is lowered by the lattice defects brought on by the decrease in oxygen vacancies at BO_6 octahedral. The primary variations in the optical energy band gap may be connected to factors, such as the synthesis circumstances, synthesis method, and form. The bandgap and temperature change are inversely correlated. It is expected that more symmetry will increase the bandwidth of the filled and vacant bands and reduce the bandgap [7].

Table 5. UV-Visible analysis for $BiFeO_3$ annealed at different temperature compared to previous studies.

This study			
Temperature (˚C)	**E_G (eV)**	**λ_{max} (nm)**	
180	2.9	475.7	
400	2.7	446.8	
600	2.5	373.5	
800	2.4	356.3	
Previous studies			
Temperature (˚C)	**E_G (eV)**	**λ_{max} (nm)**	**No. of reference**
500	2.32	421	[4]
200-500	2.73-2.61	300-400	[6]
550	3.23-2.85	300-450	[7]
150-650	2.56-2.2	300-600	[8]

3.4. An examination of magnetic characteristics

A vibrating sample magnetometer (VSM) operating at room temperature is used to examine the magnetic characteristics of the bismuth ferrites. The hysteresis loops of $BiFeO_3$ ferrite have narrower loops, which indicates soft magnetic characteristics (Figure 6). It is also commonly recognized that the presence of Fe^{3+} and an excess of O vacancies gives the $BiFeO_3$ nanoparticles their magnetic properties [8].

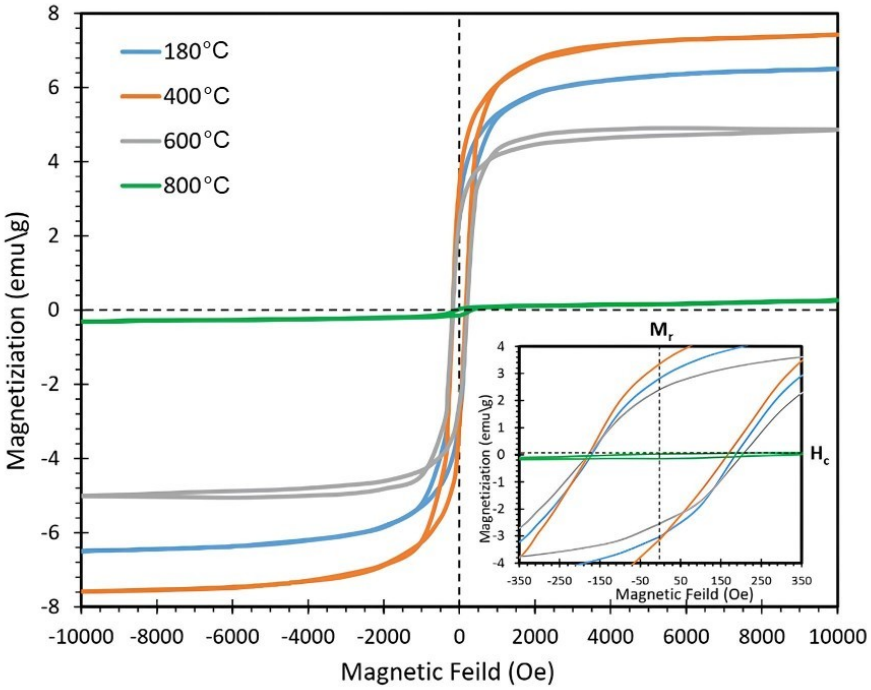

Figure 6. Hysteresis loops of $BiFeO_3$ nanoparticles prepared at 180 ˚C and annealed at 400, 600 and 800 °C.

The saturation magnetization (M_s) and coercivity (H_c) and remanence (M_r) values are obtained from the hysteresis loops (as shown in the figure inset) and listed in Table 5. The coercive field decreases at an annealing temperature of 400 °C, which corresponds to H_c = 169 Oe. Subsequently, H_c increases with rising annealing temperatures, which is attributed to changes in magnetic anisotropy because of changes in particle size. As for the saturation magnetization (M_s) values, we notice that they rise at 400 °C and then decrease. This behavior aligns with the findings of a previous study, which revealed that: $BiFeO_3$ nanoparticles synthesized at various calcination temperatures have saturation magnetization (M_s) values of 0.36 emu/g, 5.56 emu/g, 5.57 emu/g, and 0.32 emu/g for 650 °C, 550 °C, 450 °C, and 150 °C, respectively [8].

The low amounts of O–Fe–O and Fe–O bond formation are expected to contribute to the sample's low M_s value when it was calcined at 180 °C. Additionally, at a higher annealing temperature (400 °C), a notable increase occurred in M_s value. The O-Fe-O and Fe-O bonds in $BiFeO_3$ nanoparticles is likely to be the main cause of this sudden rise in the M_s value. However, at 800 °C, the magnetization value decreased again. At this time, it is likely to be attributed to the higher Bi-Fe bond length and the higher angle of O-Fe-O and Fe-O-Fe links bond [1,3]. $BiFeO_3$ nanoparticles annealed at 800 °C were found to be ferromagnetic, as demonstrated by the value of M_s = 0.25 emu/g. Its application as a magnetically separable catalyst in organic processes was further improved by the observation that the magnetization saturation value was sufficient to extract the $BiFeO_3$ nanoparticles from the reaction mixture using a powerful magnet [29].

Equation 6 is used to calculate the moment of magnetization in the Bhor magneton, and the results are shown in Table 5.

$$\mu_b = \frac{[M]M_s}{N_A\ \mu_B} \times 10^{-3} \tag{6}$$

Where: M_s: saturation magnetization in unit emu/g, [M] is Molecular Weight of bismuth ferrite measured by gm/mol. μ_B: Bohr Magneton is equal to 9.274 ×10−24 J/T. N_A: the Avogadro Number N_A = 6.022× 10^{23} mol^{-1}. 1 emu = 10^{-3} J/T is conversion factor [29]. According to Table 6, the M_r values derived from the hysteresis loops were 2.83, 3.37, 2.42, and 2.99 emu/g for T = 180, 400, 600, and 800 °C, respectively.

Table 6. The magnetic characteristics of $BiFeO_3$ nanoparticles prepared at 180 °C and annealed at 400, 600 and 800 °C.

Temperatures (°C)	M_s **(emu/g)**	M_r **(emu/g)**	H_c **(Oe)**	**K×10^3 (J/m^3)**	μ_i	μ_b
180	6.49	2.83	189	7.7	13.78	0.33
400	7.42	3.37	169	7.9	17.84	0.38
600	4.87	2.42	210	6.4	10.28	0.25
800	0.25	0.05	320	5	0.07	0.013

The magneto-crystalline anisotropy constant can be found using coercivity and saturation magnetization in Equation 7 [11]:

$$H_c = \frac{2\ K}{\mu_0 M_s} \tag{7}$$

Where: K anisotropy constant and μ_0 is free space permeability. By using the magnitudes of K the initial permeability calculated from equation [11]:

$$\mu_i = \frac{D_{cs} M_s^2}{\sqrt{K}} \tag{8}$$

Here: μ_i is the initial permeability, M_s is the Saturation Magnetization, D_{cs} is the crystallite size and K is the anisotropy constant in J/m^3. All these values are listed in Table 6. Elevated temperature greatly affects the magnetic properties of bismuth ferrite. When the annealing temperature increases above 400 °C, the magnetization decreases. Magnetic ordering may disappear completely above the Néel temperature (T_N = 370 °C). Increasing the annealing temperature may lead to a magnetic phase transition where bismuth ferrite transforms from antiferromagnetic to paramagnetic at temperatures higher than the Néel and Curie temperatures. The influence of temperature on the crystalline structure transforms from the rhombohedral phase to the cubic phase or another phase, and thus the exchange interactions between iron ions may change or weaken. This causes an alteration in the strength of magnetic behavior. Elevated temperature leads to a decrease in the mutual interactions between electric and magnetic fields, thus weakening the multiferroicity High temperatures cause the magnetism in $BiFeO_3$ samples to weaken due to increased thermal disorder. Additionally, the formation of secondary phases due to bismuth volatilization causes magnetism to decrease and the hysteresis loop to almost disappear [8].

$BiFeO_3$ nanoparticles are prepared using sol-gel method at 180 °C and processed at different annealing temperatures as a route to tune the properties for electronic and optoelectronic applications. Structural analysis

revealed the preservation of the rhombohedral R3c structure across all samples. This confirms that the annealing temperature caused no disturbance to the structural stability of $BiFeO_3$. This is vital to maintain the ferroelectric characteristics of these compounds. Raman spectroscopy confirmed the preservation of the characteristic $BiFeO_3$ structure in these nanoparticles. Variance in the lattice parameters with different annealing temperatures suggest improved crystal ordering. This can enhance the charge transport of $BiFeO_3$ nanoparticles. The optical bandgap decreased from 2.9 eV to 2.4 eV with increasing annealing temperature. This confirms the enhanced crystalline ordering of $BiFeO_3$ nanoparticles. Such feature is attractive for photo-responsive devices and applications. The change of the optical bandgap with different annealing temperatures enables tailoring these nanoparticles for various needs. The saturation magnetization decreased with higher annealing temperatures. This indicates that $BiFeO_3$ nanoparticles can be optimized to have a range of functionalities that accommodate both photoelectric and magnetoelectric needs. The balance between optical performance and magnetic ordering in $BiFeO_3$ nanoparticles is possible by controlling the processing conditions of the sol-gel method and annealing temperature.

5. Conclusions

$BiFeO_3$ nanoparticles were prepared through the sol-gel process at a temperature of 180 °C and annealed at temperatures of 400, 600, and 800 °C to examine the effect of the annealing temperature on their properties. The structural analysis indicated that the resultant powder across all sample had a rhombohedral structure with space group R3c. The analysis also revealed an increase in the crystallite size and lattice constants with increasing annealing temperature. This indicates improved crystallinity at higher temperatures of annealing. Raman spectroscopy confirmed the characteristic modes of $BiFeO_3$ with observable peak shifts with increasing annealing temperature. The bismuth ferrite nanoparticles highest absorption peak was at the visible spectrum. As the annealing temperature increases, the energy bandgap dropped from 2.9 eV to 2.4 eV, which confirms the temperature-induced structural ordering and reduction of defects . The strong absorption of $BiFeO_3$ nanoparticles in the visible region is evidence of its potential use in photo-responsive applications. The hysteresis loops of $BiFeO_3$ ferrites exhibited soft magnetic characteristics and a decrease in magnetic saturation with higher annealing temperatures. These results indicate that annealing temperature is a vital factor in determining the structural, optical and magnetic properties of $BiFeO_3$ nanoparticles. This processing-properties relationship supports their use in optoelectronic and photocatalytic applications that require controlled multifunctionality.

Author Contributions: All authors have read and approved the final manuscript. All authors contributed to editorial changes in the manuscript. All authors have participated sufficiently in the work and agreed to be accountable for all aspects of the work.

Availability of Data and Materials: The datasets used and analyzed during the current study are available from the corresponding author on reasonable request.

Funding: This research received no external sources of funding.

Declaration of AI and AI-assisted Technologies in the Writing Process: AI tools were not used in drafting of the manuscript, production of images or graphical elements of the paper, or in the collection and analysis of data.

Conflict of Interest: The authors declare no conflict of interest.

References

1. Arora, M.; Sati, P.C.; Chauhan, S.; Chhoker, S.; Panwar, A.K.; Kumar, M. Structural, Optical and Multiferroic Properties of BiFeO3 Nanoparticles Synthesized by Soft Chemical Route. *Journal of Superconductivity and Novel Magnetism* 2012, 26(2), 443–448. https://doi.org/10.1007/s10948-012-1761-4

2. Aishwarya, K.; Hannah Jeniffer, I.; Maruthasalamoorthy, S.; Nirmala, R.; Punithavelan, N.; Navamathavan, R. Review—State of the Art of the Multifunctional Bismuth Ferrite: Synthesis Method and Applications. *ECS Journal of Solid State Science and Technology* 2022, 11(4), 043010. https://doi.org/10.1149/2162-8777/ac627a
3. Taha, G.M.; Rashed, M.N.; El-Sadek, M.S.; Moghazy, M.A. Effect of Preheating Temperature on Synthesis of Pure BiFeO3 via Sol–Gel Method. *Nanopages* 2019; 1–11. https://doi.org/10.1556/566.2017.0010
4. Priya, A.; Geetha, D.; Siqueiros, J.; Ţălu, Ş. Tunable Optical and Multiferroic Properties of Zirconium and Dysprosium Substituted Bismuth Ferrite Thin Films. *Molecules* 2022, 27(21), 7565. https://doi.org/10.3390/molecules27217565
5. Ghahfarokhi, S.E.M.; Larki, M.R.; Kazeminezhal, I. Effect of Annealing Temperature on the Structural and Optical Properties Bismuth Ferrite (BiFeO3) Nanoparticle. *Journal of Research on Many-body Systems* 2019, 9, 179-191. https://doi.org/10.22055/jrmbs.2019.14600
6. Meena, H.K.; Meena, K.; Verma, R.; Jain, K.; Jain, S.K.; Sharma, K.B.; Tripathi, B. Tuning of Optical Properties via Annealing of Bismuth Ferrite (BiFeO3) Thin Films. Open Journal of Composite Materials, 2024, 14(03), 124–131. https://doi.org/10.4236/ojcm.2024.143009
7. Sardar, K.; Ali, K.; Altaf, S.; Sajjad, M.; Saleem, B.; Akbar, L.; Sattar, A.; Ali, Z.; Ahmed, S.; Elahi, U. Enhanced Structural and Optical Properties of Bismuth Ferrite ($BiFeO_3$) Nanoparticles. *Digest Journal of Nanomaterials and Biostructures* 2020, 15(1), 51–57. https://doi.org/10.15251/djnb.2020.151.51
8. Singh, H.; Rajput, J.K. Effect of Calcination Temperature on Magnetic, Structural, Thermal and Optical Properties of BFO-T Nanoparticles. *SN Applied Sciences* 2020, 2(8), https://doi.org/10.1007/s42452-020-3140-2
9. Joorabchi Bokharaei, Z.; Askarizadeh, E.; Khoobi, M.; Karimi, M.; Masjedi, A. BiFeO3@BSA-Gd2O3 Nanoparticles as Contrast Agent for Dual Imaging. *Nanomedicine Research Journal* 2025, 9(3), 274-282. https://doi.org/10.22034/nmrj.2024.03.005
10. Layek, S.; Verma, H.C. Magnetic and Dielectric Properties of Multiferroic BiFeO3 Nanoparticles Synthesized by a Novel Citrate Combustion Method. *Advanced Materials Letters* 2012, 3(6), 533– 538. https://doi.org/10.5185/amlett.2012.icnano.242
11. Jaber, N.A.; Zaki, A.M.; Fadhil, G.A. Study Phase Structure, Cation Distribution and Magnetic Properties of Cobalt, Magnesium and Copper Ferrites. *Surface Review and Letters* 2025, 2550103. https://doi.org/10.1142/s0218625x25501033
12. Tuama, A. Q.; Fadhil, G. A.; Al-dulaimi, W. A. S. Structural and photocatalytic insights into anatase TiO_2 nanostructure for dye degradation. *Experimental and Theoretical Nanotechnology* 2026, 10(1), 25–36. https://doi.org/10.56053/10.1.25
13. Petrukhin, D.; Salnikov, V.; Nikitin, A.; Sidane, I.; Slimani, S.; Alberti, S.; Peddis, D.; Omelyanchik, A.; Rodionova, V. Effect of Bismuth Ferrite Nanoparticles on Physicochemical Properties of Polyvinylidene Fluoride-Based Nanocomposites. *Journal of Composites Science* 2024, 8(8), 329. https://doi.org/10.3390/jcs8080329
14. Ablat, A.; Wu, R.; Mamat, M.; Li, J.; Muhemmed, E.; Si, C.; Wu, R.; Wang, J.; Qian, H.; Ibrahim, K. Structural analysis and magnetic properties of Gd doped $BiFeO_3$ ceramics. *Ceramics International* 2014, 40(9), 14083–14089. https://doi.org/10.1016/j.ceramint.2014.05.137
15. Hegab, A.F.; Ahmed Farag, I.S.; EL-Shabiny, A.M.; Nassaar, A.M.; Ramadan, A.A.; Moustafa, A.M. Role of Sr doping on transport and magnetic properties of bismuth ferrite in correlation with defect formation. *Journal of Materials Science: Materials in Electronics* 2017, 28(19), 14460–14470. https://doi.org/10.1007/s10854-017-7308-5
16. Srinivas, V.; Raghavender, A.T.; Kumar, K.V. Structural and Magnetic Properties of Mn Doped $BiFeO_3$ Nanomaterials. *Physics Research International* 2016, 2016(1), 1–5. https://doi.org/10.1155/2016/4835328
17. Leal-Zayas, J.C.; Vargas-Ortiz, R.Á.; Almaral-Sánchez, J.L.; Mendivil-Escalante, J.M.; Silva-González, R.; Moya-Canul, K.M.; Peña-Flores, J.I.; Yáñez-Limón, J.M. Study of the physical properties of $BiFeO_3$ films obtained by RF sputtering using a homemade target. *Boletín de La Sociedad Española de Cerámica y Vidrio* 2025, 64(2), 86–95. https://doi.org/10.1016/j.bsecv.2024.10.001
18. Wu, S.; Zhang, J.; Liu, X.; Lv, S.; Gao, R.; Cai, W.; Wang, F.; Fu, C. Micro-Area Ferroelectric, Piezoelectric and Conductive Properties of Single $BiFeO_3$ Nanowire by Scanning Probe Microscopy. *Nanomaterials* 2019, 9(2), 190. https://doi.org/10.3390/nano9020190

19. Sayed, R.; Hassanien, A.; Hashim, H.; Mabied, A.; Ramadan, A.; Soltan, S. Investigation of the temperature-dependent functioning of $BiFeO_3$ as a ferroelectric material through X-ray diffraction analysis. *Applied Physics A* 2024, 131, 30. https://doi.org/10.1007/s00339-024-08101-6
20. Jalandhara, D.; Singh, G.; Yadav, K. Effect of sintering temperature on the optical properties of $BiFeO_3$ nanoparticles. *AIP Conference Proceedings* 2016, 1728 (1), 020437. https://doi.org/10.1063/1.4946488
21. Momin, A.A.; Zubair, M.A.; Islam, M.F.; Hossain, A.K.M.A. Enhance magnetoelectric coupling in $xLi_{0.1}Ni_{0.2}Mn_{0.6}Fe_{2.1}O_{4-(1-x)}BiFeO_3$ multiferroic composites. *Journal of Materials Science: Materials in Electronics* 2019, 30(14), 13033–13046. https://doi.org/10.1007/s10854-019-01665-7
22. Zhang, F.; Zeng, X.; Bi, D.; Guo, K.; Yao, Y.; Lu, S. Dielectric, Ferroelectric, and Magnetic Properties of Sm-Doped $BiFeO_3$ Ceramics Prepared by a Modified Solid-State-Reaction Method. *Materials* 2018, 11(11), 2208. https://doi.org/10.3390/ma11112208
23. Stojadinović, B.; Djokić, D.M.; Paunović, N.; Živković, I.; Ćirić, L.; Kusigerski, V.; Dohčević-Mitrović, Z. Unvailing the spin–phonon coupling in nanocrystalline $BiFeO_3$ by resonant two-phonon Raman active modes. *Materials Science and Engineering: B* 2021, 274, 115444. https://doi.org/10.1016/j.mseb.2021.115444
24. Viet Thang, D.; Manh Hung, N.; Phuong Thao, N.; Cao Khang, N.; Thi Mai Oanh, L.; Thi Cam Linh, N.; Dinh Tu, B. Effect of Eu Doping on Structural, Optical and Magnetic Properties of $BiFeO_3$ Materials. *VNU Journal of Science: Mathematics – Physics* 2022, 38(1). https://doi.org/10.25073/2588-1124/vnumap.4640
25. Wang, J.; Luo, L.; Han, C.; Yun, R.; Tang, X.; Zhu, Y.; Nie, Z.; Zhao, W.; Feng, Z. The Microstructure, Electric, Optical and Photovoltaic Properties of $BiFeO_3$ Thin Films Prepared by Low Temperature Sol–Gel Method. *Materials* 2019, 12(9), 1444. https://doi.org/10.3390/ma12091444
26. Juwita, E.; Sulistiani, F.A.; Darmawan, M.Y.; Istiqomah, N.I.; Suharyadi, E. Microstructural, optical, and magnetic properties and specific absorption rate of bismuth ferrite/SiO2 nanoparticles. *Materials Research Express* 2022, 9(7), 076101. https://doi.org/10.1088/2053-1591/ac804e
27. Dybov, V.A.; Kalinin, Y.E.; Kamynin, A.A.; Kashirin, M.A.; Makagonov, V.A.; Nikonov, A.E.; Serikov, D.V.; Sitnikov, A.V. Electrical and optical properties of thin-film bismuth ferrite. *Technical Physics* 2022, 67(12), 1702. https://doi.org/10.21883/tp.2022.12.55208.182-22 .
28. Ayala, Z.B.; Peñalva, J.; Hernández, J.M.; Loro, H.; Eyzaguirre, C. Study of the optical and photovoltaic properties in nanoparticles of $BiFeO_3$. *Journal of Physics: Conference Series* 2020, 1558(1), 012010. https://doi.org/10.1088/1742-6596/1558/1/012010
29. Saleh, H.; Ali, K.; Raheem, A. The Deflection of the Magnetic Ring for the Magnetic System $Co_xCu_{1-x}Fe_2O_4$. *Journal of Engineering and Applied Sciences* 2019, 14(11), 3620-3624. https://doi.org/10.36478/JEASCI.2019.3620.3624